back

A SYSTEM FOR UNSTEADY PRESSURE MEASUREMENTS REVISITED

H. Tijdeman[1] **and R.M.E.J. Spiering**[1]

[1] University of Twente, Faculty of Engineering Technology
P.O.Box 217, 7500 AE Enschede, The Netherlands
e-mail: h.tijdeman@ctw.utwente.nl and r.m.e.j.spiering@ctw.utwente.nl

Key words: Acoustics, Sound Absorption, Unsteady pressure measurements, Viscothermal wave propagation

Abstract. An overview is presented of some recent developments in the field of the design of effective sound absorbers. The first part deals with the application of so-called coupled tubes. For this purpose use is made of a system originally applied for unsteady pressure measurements on oscillating wind tunnel models. The second part deals with an extension of the theory of tubing systems to thin air layers, trapped between flexible walls.

1 BACKGROUND

In the early sixties Bergh [1] introduced at the NLR (National Aerospace Laboratory, Amsterdam) a new method to measure detailed unsteady pressure distributions on harmonically oscillating wind tunnel models. Key feature was the use of the same tube-scanning valve systems as commonly applied for steady pressure measurements. This avoided the use of a large number of in-situ transducers, which were hardly available and very expensive at that time. Moreover steady and unsteady tests could be performed simultaneously on the same models. At about the same time Laschka [2, 3] published his new theory on the air loads on oscillating surfaces. The unique coincidence of a new theory and an affordable measuring technique led to a fruitful combination of piloting research on unsteady aerodynamics, reflected in two classical papers by the aforementioned authors, published at the same congress in 1963 [1, 4]. See Figure 1.

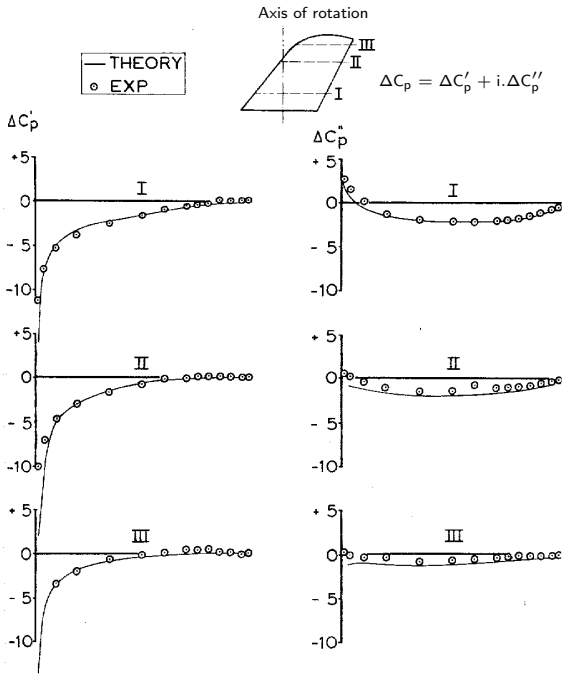

Figure 1: Unsteady pressure distributions on a fin oscillating in yaw-motion [1]

For measuring the harmonically oscillating part of the pressures at the surface of the model one has to account for the transfer function of the tubing system. This system causes a change in both amplitude and phase angle between the unsteady pressure at the surface and the unsteady pressure as felt by the transducer. The transfer function not only depends on the dimensions of the tubes, but also on the mean temperature and the local mean pressure at the entrance of the tube on the model surface. Overall this led to

a rather complicated data reduction procedure, as sketched in Figure 2. The procedure was simplified somewhat by giving all tubes the same length. The measuring technique

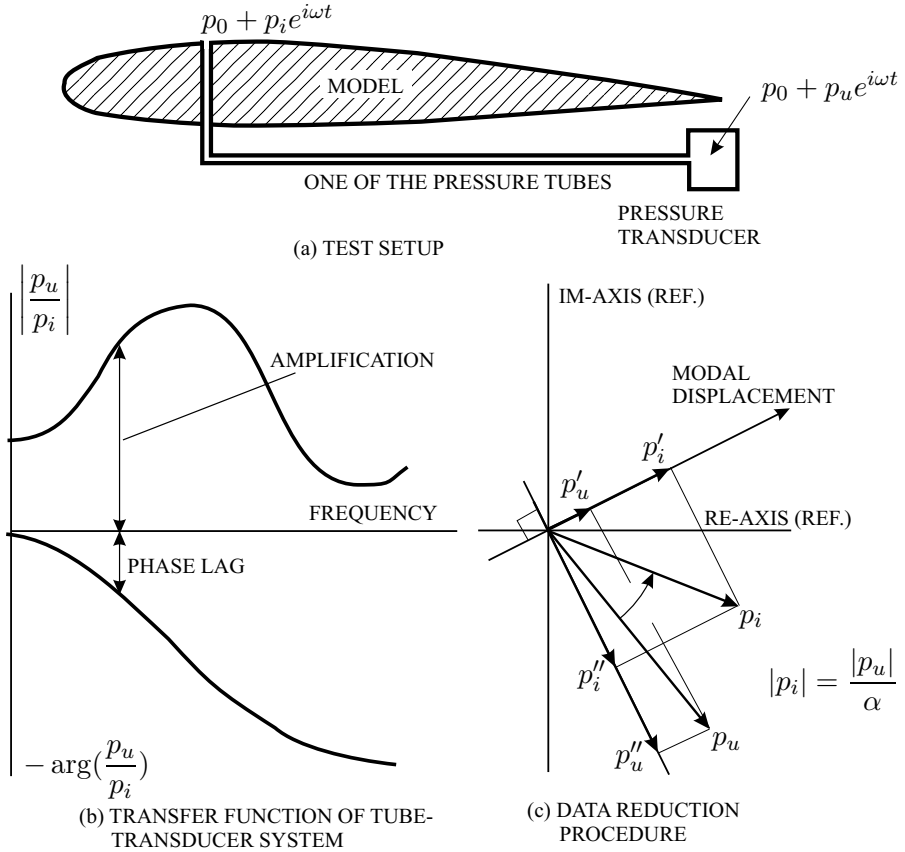

Figure 2: Data reduction procedure to compensate for the transfer function of the tubing system

was given a fundamental basis [5,6] by the development and experimental validation of a mathematical model. Essential for the propagation of sound waves through tubes is the inclusion of the effects of heat transfer and viscosity. This process is governed by the value of the so-called shear-wave number, S, defined as:

$$S = R\sqrt{\frac{\rho_0 \omega}{\mu}} \tag{1}$$

with R the radius of the tube (m), ρ_0 the mean density of gas or fluid (kg/m^3), ω the angular frequency (rad/s) and μ the dynamic viscosity (Pa s).
For low values of S the physical process inside the tube can be considered as isothermal, whereas at high values the process happens isentropically. It has to be noted that a low value of S not only shows up at low frequencies, but also for very narrow tubes at high frequencies.
Some characteristic examples of transfer functions are presented in Figure 3.
One must be aware (see Figure 3.c) that at very high local mean velocities, as happens for instance around airfoils operating in transonic flow an important influence of the "grazing" flow on the transfer function of tubing systems occurs, which has to be accounted for [7,8].

It is interesting to note how the method to determine the transfer functions of tubing systems and probes has spread out to a variety of applications, besides the field of aero-

elasticity. It mainly concerns test conditions in which the sensors, for instance because of a hostile environment, have to be placed at a certain distance from the source.
Examples are the application in the atomic center of Los Alamos [Watts, 9], in fluidized-bed furnaces [van Ommen, 10], pressure probes for jet engines [Brouckaert et.al., 11, 12] and scramjets [Heller, Parrot, 8, 13], applications to re-entry vehicles under rarified flow conditions and large temperature gradient [Whitmore, Jones and Thurlow, Heller, 8, 14], turbulence probes to study natural erosion problems in harsh environments [Findlater, 15], heat pipes [Rott, 16, 17] and extensions to super heated refrigerants and thermo-acoustic problems [Rodarte et.al., 18] and even piping systems for the transport of natural gas. For a number of applications the model had to be adapted or extended. For details reference is made to the mentioned publications. Some interesting extensions to larger amplitudes and the inclusion of a mean flow through the tubes can be found in [19–21].

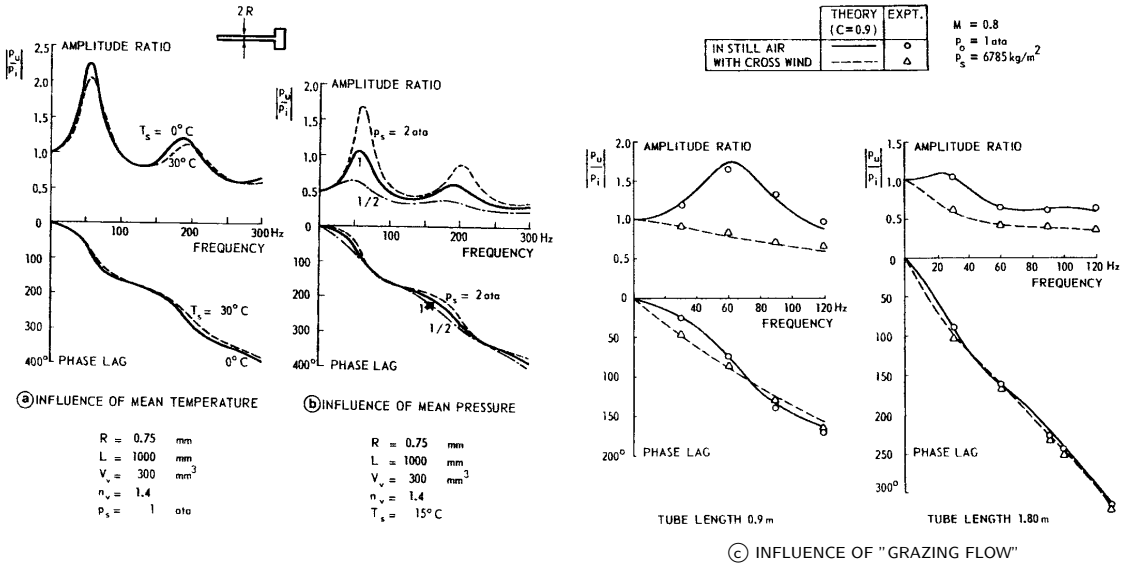

Figure 3: Examples of the transfer function of tube transducer systems

2 RESEARCH IN TWENTE

This paper addresses the work, started at the University of Twente more than thirty years after the introduction of the tubing system for unsteady pressure measurements at the NLR. We took up the modeling of viscothermal wave propagation and considered again tube-systems. This time in the reversed sense, with the aim to design acoustic dampers and sound absorbing walls. We also extended the theory to numerically simulate the effects, which the presence of thin air-layers, trapped between flexible plate-type structures, has on the vibration- and damping characteristics of such structures. It is demonstrated that such layers might have a considerable effect on lightweight structures, both with respect to eigenfrequencies and to damping.

2.1 Reversed tube systems

As mentioned we revisited the tubing system. Beltman [22,23] and Van der Eerden [24,25] considered a trapped system consisting of a series of tubes. A very efficient numerical tool has been developed and validated to design panels with optimal sound absorbing characteristics. A number of tubing-configurations have been designed with optimal sound absorption in a relatively wide and predefined frequency range.

In Figure 4 the sound absorption coefficient of a sample with ordinary equal quarter lambda oscillators is shown. The location and width of the peak are very well predicted. Of more practical interest are configurations with so-called coupled tubes with different dimensions, as for example the ones presented in Figures 5 - 8.
Evidently a much wider frequency range can be created in which a very effective sound absorbtion is obtained.
The predicted characteristics agree very well with the measurements, implying that we have an excellent method in hand to design effective acoustic characteristics in a prescribed frequency band. The method lends itself very well for an optimization procedure. It has to be noted that in the calculations the actual lengths of the tubes are used with a virtual addition to account for inlet effects. This corrections are taken from the literature [Bies and Hansen, 26] (R is the tube radius, a is the distance between the centers of the tubes, equally spaced).

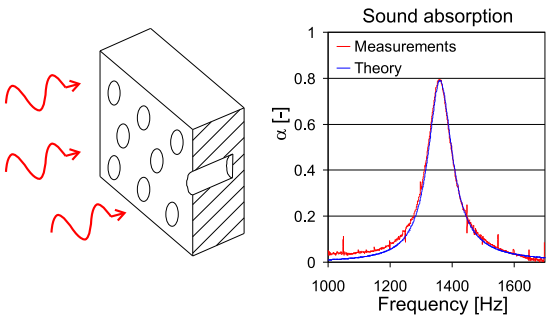

Figure 4: Absorption coefficient of a wall with one type of quarter lambda oscillators [24]

$$L_{\text{effective}} = L_{\text{actual}} + \frac{8\,R}{3\,\pi}\left(1 - 0.44\frac{R}{a}\right) \quad \text{with } a > 2R \tag{2}$$

At the wall the impedance, Z_{wall}, is defined as the quotient of the local pressure and the normal particle velocity. In general the impedance is a complex number. The reflection

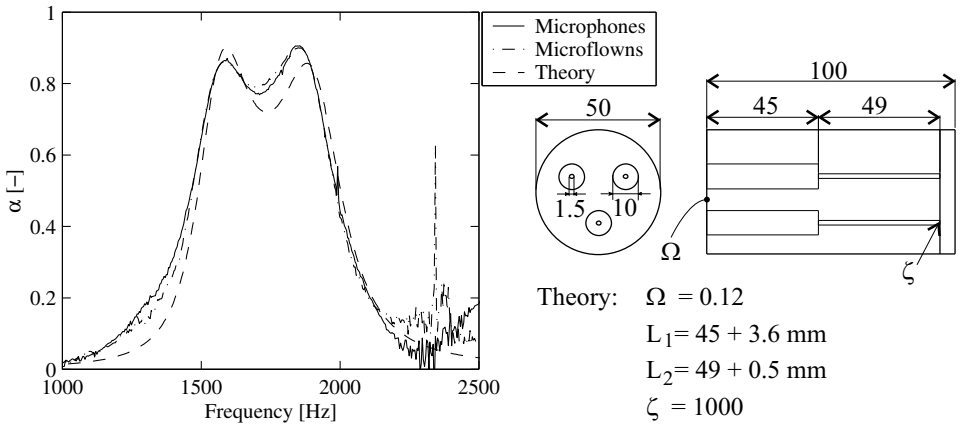

Figure 5: Sound absorption coefficient of a sample with three coupled tubes [24]

coefficient at the wall, R_{wall}, is the ratio of the reflected and incident wave. It can be derived [24] that:

$$R_{\text{wall}} = \frac{Z_{\text{wall}} - \rho_0 c_0}{Z_{\text{wall}} + \rho_0 c_0} \tag{3}$$

Where ρ_0 represents the mean density and c_0 the sound velocity of air at the prevailing conditions. Finally the sound absorption coefficient, α, is defined as the fraction of incident

sound energy that is dissipated at the wall. It can be expressed in the reflection coefficient as follows:

$$\alpha = 1 - |R_{\text{wall}}|^2 \tag{4}$$

The wall impedance, reflection coefficient as well as the absorption coefficient are all frequency dependant. The value Ω corresponds with the so-called porosity, defined as:

$$\Omega = \frac{1}{A_{\text{wall}}} \sum_{i=1}^{n} A_{\text{tube } i} \quad i = 1, 2, \cdots, n \tag{5}$$

Here A_{wall} represents the considered area of the wall, $A_{\text{tube } i}$ the inner cross-section area of the i^{th} tube and n the number of tubes. The validation tests have been performed

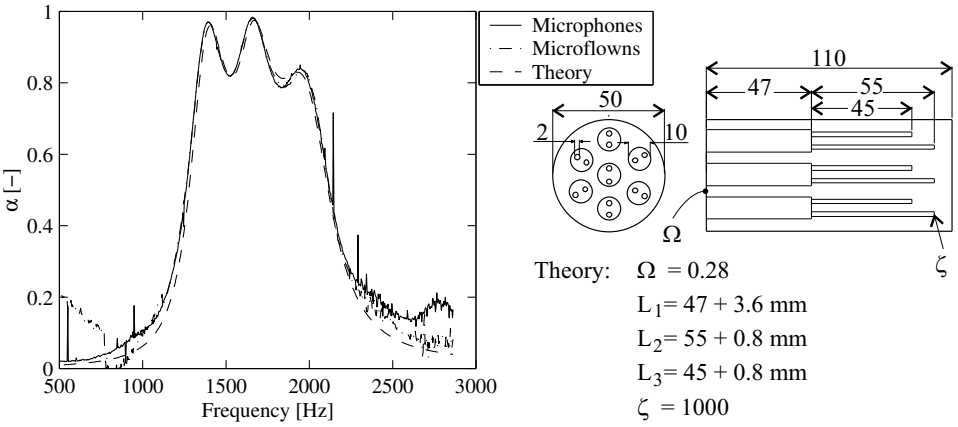

Figure 6: Sound absorption coefficient of a sample with seven coupled tubes [24]

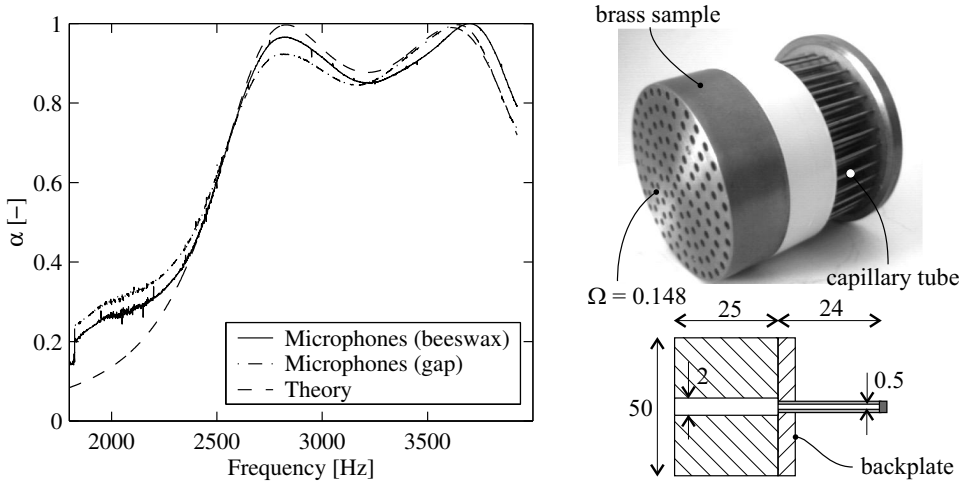

Figure 7: Sound absorption coefficient of a sample with coupled tubes [24]

in an impedance tube, with both small microphones and ditto microflowns, mems-type devices [27] with which particle velocity perturbation is directly measured instead of pressure perturbation.

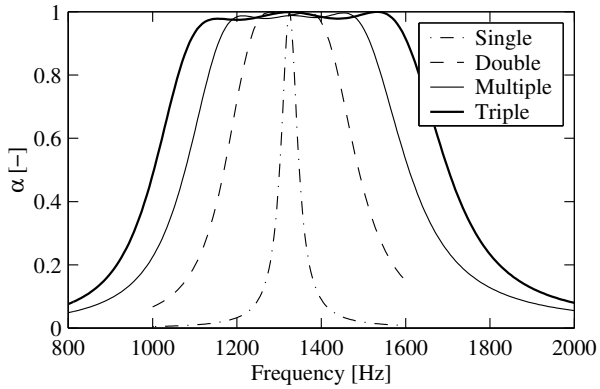

Figure 8: Sound absorption coefficients of several samples with coupled tubes [24]

It is also possible to distribute a very large number of tubes with random chosen dimensions in a random way in a structure and to compute the sound absorption of such a network. See Figure 9(a). The predicted results correspond quite well with the predictions by the semi-experimental theory of Delany & Bailey [28]. See Figure 9(b). The number within the round brackets represents the flow resistivity in Nsm^{-4}. It is noted that in the "tube theory" the flow resistivity can be computed by considering the system at very low frequency.

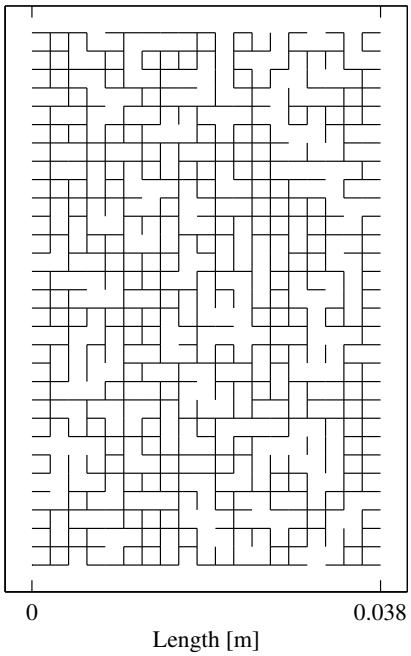

(a) Random network of coupled tubes

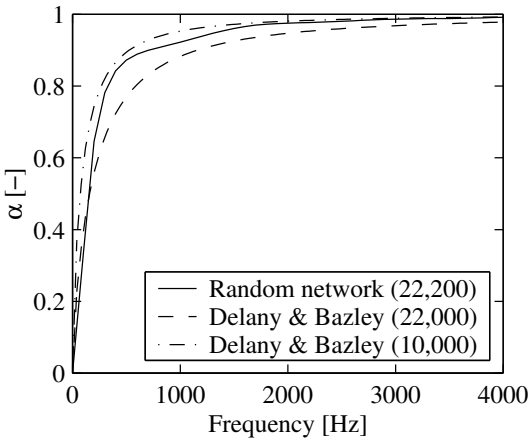

(b) Sound absorption coefficient of a network compared with semi-empirical predictions

Figure 9: Example of a network with a random distribution of coupled tubes [24]

In the Appendix a new FEM-like approach has been presented to determine the dynamic behavior, both in the direct sense (pressure measurements) as in reversed sense of complex, branched tubing systems. This formulation with which more complex systems can be computed than in the earlier formulation [5] is well suited for implementation on a PC. For validation purposes the example in Figure 10 showing the impedance at junction 2 of a T-shape configuration is presented. Note the difference between the results of the present model (low reduced frequency) and the results of the model without viscothermal effects.

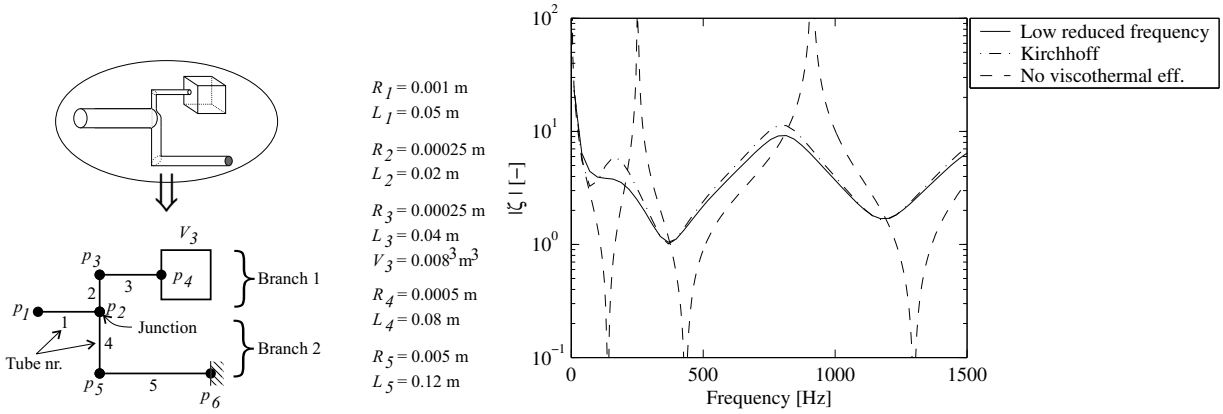

(a) A T-shape configuration of tubes

(b) Impedance (magnitude) at junction 2

Figure 10: Example of a set of coupled tubes computed with the method of the Appendix [24]

2.2 Thin air layers (squeeze film damping)

In a second application we considered thin air-layers, as occurring in the case of plate-type structures, backed by a cavity. For this purpose a new mathematical model and a corresponding finite element formulation have been developed [22, 29, 30]. The fluid-

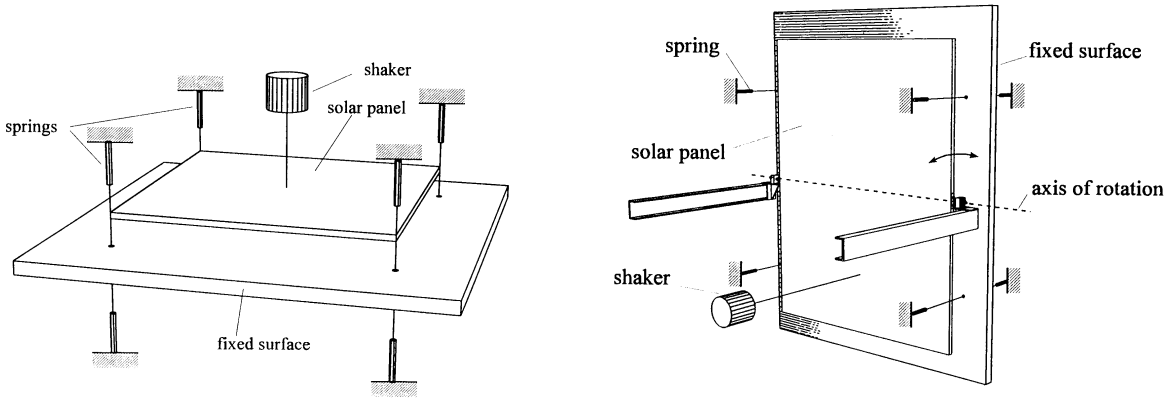

(a) Setup for heave motion

(b) Setup for pitch motion

Figure 11: Test setups for validation of squeeze film theory [23]

dynamics part of the model is validated with the help of measurements on a solar panel, suspended in springs and oscillating in heave (i.e. oscillating normal to its surface) and in pitch (i.e. oscillating around an axis of rotation) in the vicinity of a fixed bottom plate (Figure 11). In this way a very low shear wave number could be obtained, without going to a miniature type test up. The added mass and extra damping created by the motion of the air has been determined by measuring the phase-resonance frequency (90 degrees phase shift between excitation and response) and damping of the solar panel for various thicknesses of the air layer. The narrow air gap (width h_0) between the panel and the fixed plate is shown to have a tremendous effect on the phase-resonance frequency and damping (Figure 12).

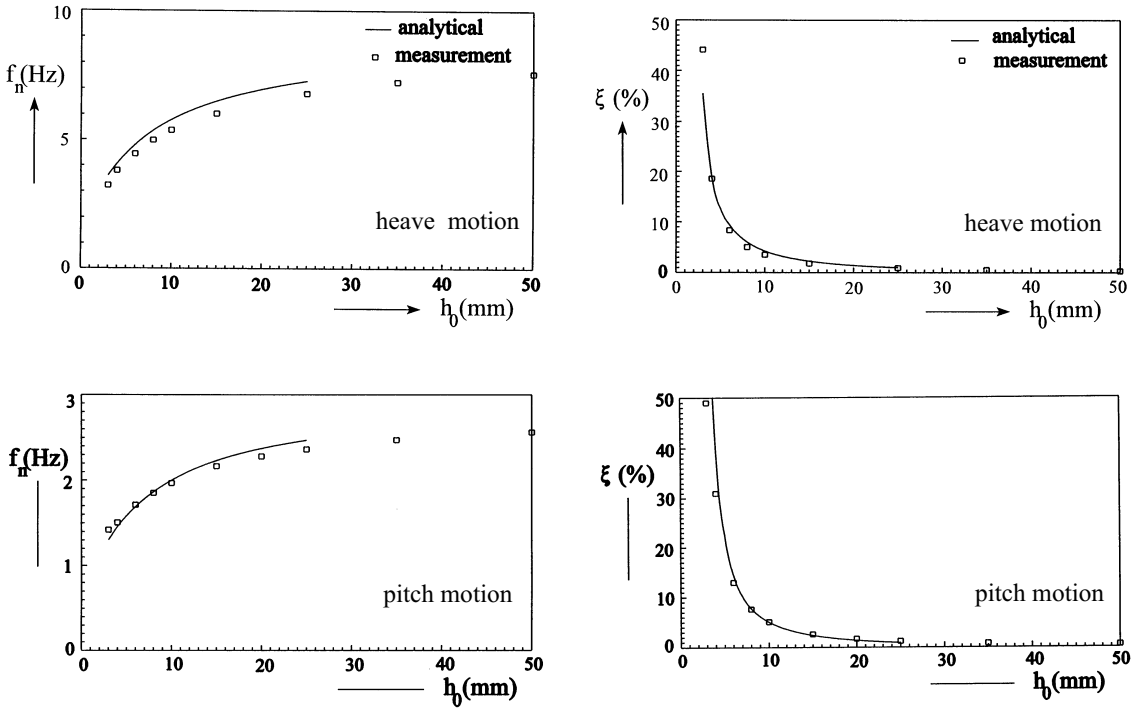

Figure 12: Result of the experiments with heave and pitch motion [23]

This is reflected also if we consider the results in terms of added mass and damping, see Table 1.

HEAVE		PITCH	
mass of panel	2.54 kg	moment of inertia	1.64 kg m^2
dimensions	$0.98 * 0.98$ m	dimensions	$1.67 * 1.29$ m
added mass	22 kg	added moment of inertia	5.5 kg m^2
damping value	35 %	damping value	> 60 %

Table 1: Added mass and damping coefficient for a gap width of 3 mm

Placing small obstacles in the air gap can create even more damping [22, 31, 33].

To validate the fluid-structure interaction part of the mathematical model a relatively simple experiment has been conducted in which a narrow air layer is considered in a two-way coupling between the air layer and a flexible plate [22, 23, 30, 31]. For this purpose use was made of an airtight box with a flexible aluminium cover plate of 1 mm thickness (Figure 13). The gap width (h_0) could be varied between 1 and 50 mm. The plate is

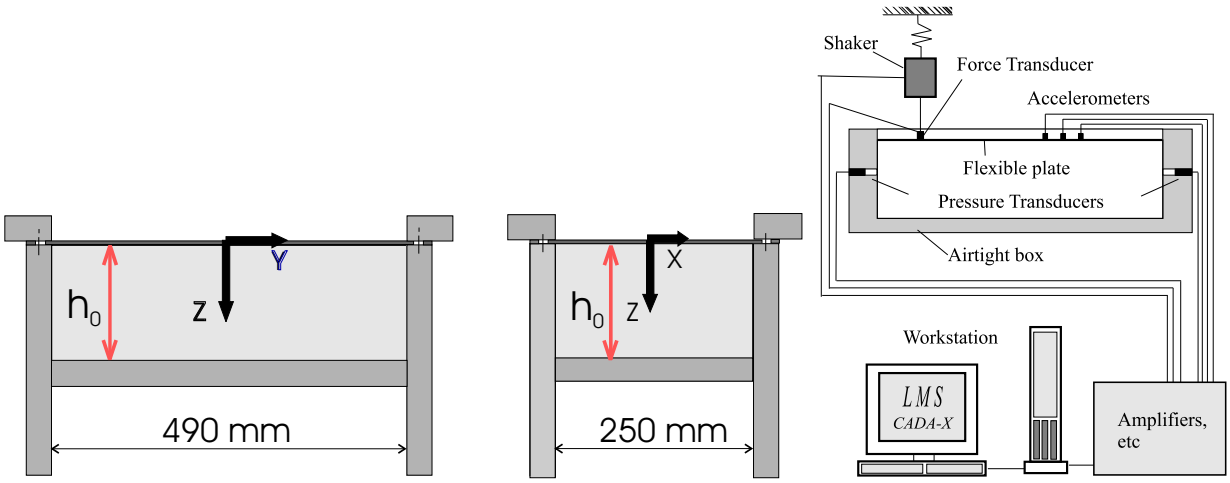

(a) Dimensions of the test box

(b) Setup of the test box

Figure 13: The test setup

excited with a shaker and the point of excitation was chosen in such a way that it did not coincide with a node of one of the eigenmodes in the applied frequency range. As in the preceding example the width of the air layer significantly effects the eigenfrequencies and damping (Figure 14). Three effects can be distinguished: additional stiffness, added mass and extra damping.

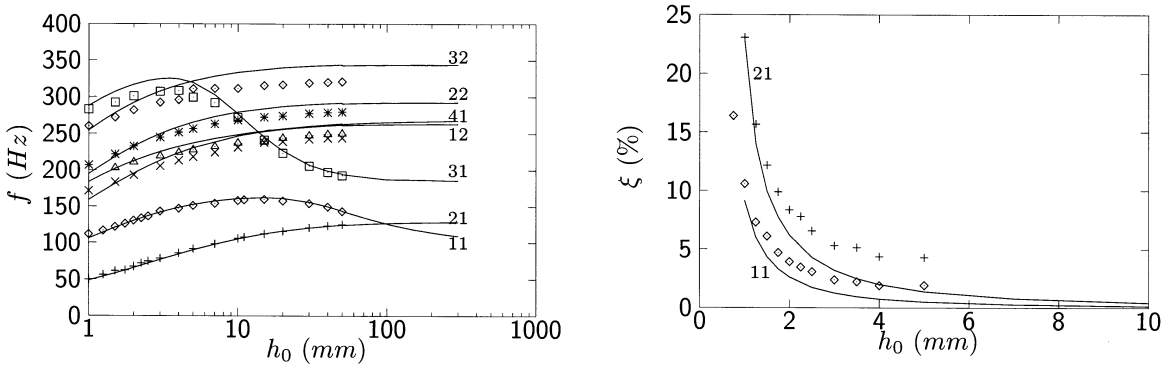

(a) Frequencies

(b) Damping

Figure 14: Effect of gap width on eigenfrequencies and damping of the flexible plate

For symmetrical vibration modes the "extra spring stiffness" becomes more and more important when the gap becomes smaller (raising of the eigenfrequency). Additional mass

plays a role when the air in the gap is pumped back and forth (pumping effect) as happens for asymmetrical vibration modes of the cover plate (lowering of the eigenfrequency). Both effects are depicted in Figure 15.

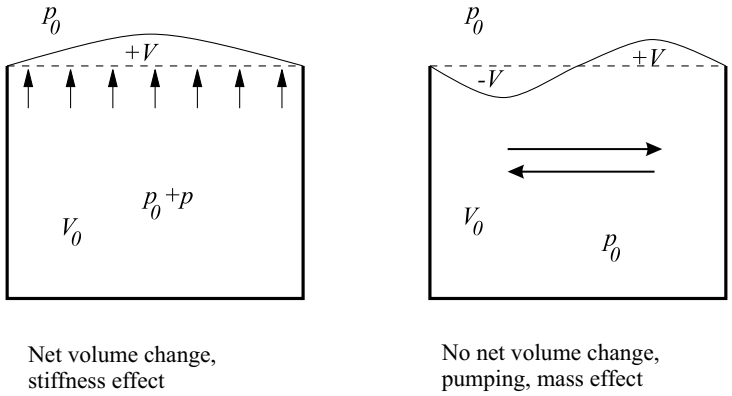

Figure 15: Stiffness and pumping effect

The method described above has been applied to predict the dynamic behavior of stacked solar panels, folded against a satellite. This behavior is of crucial importance during the launch phase. A corresponding experimental setup is depicted in Figure 16.
Another topic which can be treated is the dynamic behavior of panels, backed by a narrow cavity as occurs for instance on re-entry vehicles. Further applications concern the design of double wall panels to reduce structure born sound transmission [31, 32].

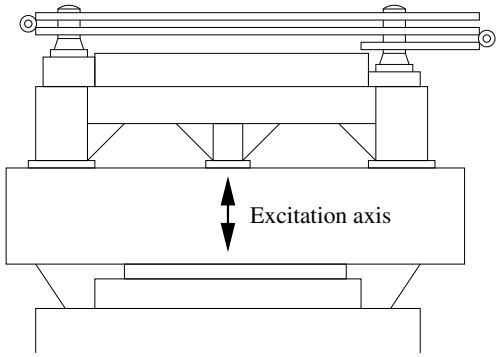

Figure 16: Setup of solar panels experiment

An interesting way to increase damping of double wall panels is to combine thin air layers with reversed tube systems. Experiments have shown that this is a promising combination since then both symmetrical and asymmetrical vibration modes can be passively damped [24, 31].

3 CONCLUDING REMARKS

An overview is given of some recent developments at the University of Twente on passive systems for sound absorption and vibration damping. Use is made of a method, originally applied for unsteady pressure measurements on oscillating airfoils. The method has been extended to treat thin air layers as well.

APPENDIX A FEM-like tube model

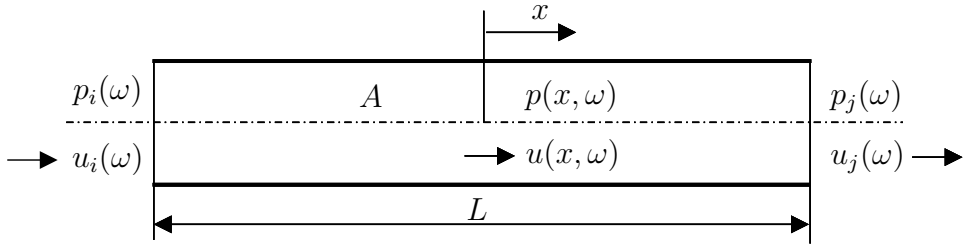

Figure 17: Prismatic tube with length L

Starting-point is the equations for distribution of the complex amplitudes of the pressure (6) and the averaged velocity (7) perturbation in a prismatic tube, viscothermal effects included:

$$p(x,\omega) = \left\{ C_1 \cdot \exp\left(\Gamma(\omega)\frac{\omega}{c_0}x\right) + C_2 \cdot \exp\left(-\Gamma(\omega)\frac{\omega}{c_0}x\right)\right\} \tag{6}$$

and:

$$u(x,\omega) = -\frac{G(\omega)}{\rho_0 c_0}\left\{ C_1 \cdot \exp\left(\Gamma(\omega)\frac{\omega}{c_0}x\right) - C_2 \cdot \exp\left(-\Gamma(\omega)\frac{\omega}{c_0}x\right)\right\} \tag{7}$$

The parameters $\Gamma(\omega)$ and $G(\omega)$ are dependent on angular frequency ω (rad/s) and the shape of the cross-section of the tube. It can be derived that [5, 6, 22, 24]:

$$\begin{aligned} &\Gamma(\omega) = \sqrt{\frac{\gamma}{F_c(S_{(\omega)})\, n(\omega)}} \quad ;\; G(\omega) = \frac{i}{\Gamma(\omega)}\frac{\gamma}{n(\omega)} \quad ;\; n(\omega) = \frac{1}{1+(1-\gamma^{-1})\, F_c(S_{(\omega)})\, \sigma)} \\ &F_c(s) = \sqrt{\frac{J_2(i\sqrt{i}\, s)}{J_0(i\sqrt{i}\, s)}} \qquad ;\; S_{(\omega)} = R\sqrt{\frac{\rho_o\, \omega}{\mu}} \qquad ;\; (i = \sqrt{-1}) \end{aligned} \tag{8}$$

With ρ_0 the mean density (kg/m^3), c_0 the sound velocity (m/s), γ the ratio of the specific heats (-), C_p/C_V, $S_{(\omega)}$ the so-called shear-wave number (-), see (1), σ the square root of the Prandl number (-), R the radius of the tube (m), μ the dynamic viscosity (Pa s), and s a dummy variable (-). Further is $\Gamma(\omega)$ the viscothermal wave propagation coefficient (-), $n(\omega)$ can be interpreted as a type of polytropic coefficient (-) and $F_c(s)$ is function dependant on the shape of the cross-section of the tube, in this case circular (-).
Consider a prismatic tube with length L and cross-section area A, see Figure 17. The length coordinate is x ($-\frac{1}{2}L \le x \le \frac{1}{2}L$). The integration constants C_1 and C_2 can be expressed in the pressures in the end points of the tube, $p_i = p(-\frac{1}{2}L, \omega)$ and $p_j = p(\frac{1}{2}L, \omega)$. The relations (6) and (7) now can be rewritten in:

$$p(\xi,\omega) = \frac{1}{\sinh(\kappa)}\left\{ p_i \cdot \sinh\left(\kappa\cdot(\tfrac{1}{2}-\xi)\right) + p_j \cdot \sinh\left(\kappa\cdot(\tfrac{1}{2}+\xi)\right)\right\} \tag{9}$$

and:

$$u(\xi,\omega) = -\frac{G(\omega)}{\rho_0 c_0}\frac{1}{\sinh(\kappa)}\left\{ p_i \cdot \cosh\left(\kappa\cdot(\tfrac{1}{2}-\xi)\right) - p_j \cdot \cosh\left(\kappa\cdot(\tfrac{1}{2}+\xi)\right)\right\} \tag{10}$$

with:

$$\kappa = \Gamma(\omega)\frac{\omega}{c_0}L \quad \text{and} \quad \xi = \frac{x}{L} \tag{11}$$

The mass flow perturbations in the end points of the tube (inward directed) expressed in the velocities are:

$$Q_i = \rho_0 A \cdot u(-\tfrac{1}{2}, \omega) \;\; ; \;\; Q_j = -\rho_0 A \cdot u(\tfrac{1}{2}, \omega) \tag{12}$$

With (10) then the next set of equations for one tube follows:

$$\begin{bmatrix} Q_i \\ Q_j \end{bmatrix} = \frac{A \cdot G(\omega)}{c_0 \cdot \sinh(\kappa)} \begin{bmatrix} \cosh(\kappa) & -1 \\ -1 & \cosh(\kappa) \end{bmatrix} \cdot \begin{bmatrix} p_i \\ p_j \end{bmatrix} \quad \text{or } \{Q\} = [K] \cdot \{p\} \tag{13}$$

The matrix of equation (13) can be interpreted as the (symmetric) element matrix, $[K]$, of the concerned tube, and both vectors as the element vector with mass flows, $\{Q\}$, respectively the vector with pressure degrees of freedom, $\{p\}$. If p_i or Q_i , resp. p_j or Q_j are known the remaining unknowns can be solved as a function of the frequency ω.

Subsequently a set of tubes is considered. In Figure 18 a T-configuration of three tubes connected to a volume V is depicted. The end points of the tubes are numbered 1 through 4, the tubes (elements) by $<1>$, $<2>$ and $<3>$. The dimensions of the tubes, length and cross-section, can be different. The fluid or temperature in the tubes may differ as well. The relation between the pressure perturbations in the different tubes is found in the condition that they are equal at the connection point. So:

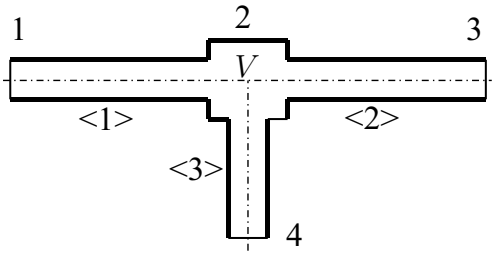

Figure 18: AT-configuration of tubes

$$p_i^{<1>} = p_1 \;\; ; \;\; p_j^{<1>} = p_V = p_i^{<2>} = p_i^{<3>} = p_2 \;\; ; \;\; p_j^{<2>} = p_3 \;\; ; \;\; p_j^{<3>} = p_4 \tag{14}$$

Furthermore the mass balance, taking in account the directions of mass flow, gives:

$$Q_j^{<1>} + Q_i^{<2>} + Q_i^{<3>} + \frac{i\omega}{c_V^2} \frac{\gamma}{n_V} V \cdot p_2 = 0 \tag{15}$$

Combined with equation (13) this results in a set with linear equations:

$$\begin{bmatrix} Q_i^{<1>} \\ 0 \\ Q_j^{<2>} \\ Q_j^{<3>} \end{bmatrix} = \begin{bmatrix} Q_1 \\ 0 \\ Q_3 \\ Q_4 \end{bmatrix} = \begin{bmatrix} K_{11}^{<1>} & K_{12}^{<1>} & 0 & 0 \\ K_{21}^{<1>} & K_{22}^{<1>} + K_{11}^{<2>} + K_{11}^{<3>} + K_V & K_{12}^{<2>} & K_{12}^{<3>} \\ 0 & K_{21}^{<2>} & K_{22}^{<2>} & 0 \\ 0 & K_{21}^{<3>} & 0 & K_{22}^{<3>} \end{bmatrix} \cdot \begin{bmatrix} p_1 \\ p_2 \\ p_3 \\ p_4 \end{bmatrix} \tag{16}$$

with:

$$K_V = \frac{i\omega}{c_V^2} \frac{\gamma}{n_V} V \tag{17}$$

The contribution of the volume V is found in the system matrix as a one by one element matrix K_V.
Several boundary conditions at the end of a tube are possible.

- The amplitude of the pressure perturbation is prescribed or zero (open end); then the mass flow perturbation is not known and has to be calculated.
- The mass flow perturbation is prescribed or zero (closed end); then the pressure perturbation is not known.

- An impedance end condition. The pressure and the velocity (outward directed) at the tube end are linear dependent:

$$\frac{p_i}{-u_i}=\frac{\rho_0 c_0}{G(\omega)}\zeta \text{ or } \frac{p_j}{u_j}=\frac{\rho_0 c_0}{G(\omega)}\zeta \;\Rightarrow\; Q_i=-\left(\frac{A\cdot G(\omega)}{c_0\zeta}\right)^{<e>} p_i \text{ or } Q_j=-\left(\frac{A\cdot G(\omega)}{c_0\zeta}\right)^{<e>} p_j \quad (18)$$

  Here $\rho_0 c_0/G(\omega)$ represents the so-called characteristic impedance in case of a duct with viscothermal wave propagation and ζ is the scaled (dimensionless) impedance. In this way a infinitely long tube (non-reflecting boundary) is simulated when $\zeta = 1$; one of the integration constants of equation (6), C_1 or C_2, becomes zero.

As an example the following boundary conditions for the T-configuration shown in Figure 18 are applied:
In point 1 the pressure is prescribed, in point 3 the tube is closed ($Q_3 = 0$) and in point 4 the impedance is given. This leads to the next set of equations:

$$\begin{bmatrix} K_{22}^{<1>}+K_{11}^{<2>}+K_{11}^{<3>}+K_V & K_{12}^{<2>} & K_{12}^{<3>} \\ K_{21}^{<2>} & K_{22}^{<2>} & 0 \\ K_{21}^{<3>} & 0 & K_{22}^{<3>}+K_Z^{<3>} \end{bmatrix} \cdot \begin{bmatrix} p_2 \\ p_3 \\ p_4 \end{bmatrix} = \begin{bmatrix} -K_{21}^{<1>}\cdot p_1 \\ 0 \\ 0 \end{bmatrix} \quad (19)$$

and: $Q_1 = K_{11}^{<1>}\cdot p_1 + K_{12}^{<1>}\cdot p_2$ (can be calculated after p_2 is found)

with:

$$K_Z^{<3>} = \left(\frac{A\cdot G(\omega)}{c_0\zeta}\right)^{<3>} \quad (20)$$

The impedance condition is found in the system matrix as an extra one by one element matrix $K_Z^{<e>}$. A special impedance-like boundary condition is obtained when a tube is closed with a piston (mass m_p), supported by a spring (stiffness constant k_p) and a damper (damping constant b_p). In this case is found:

$$K_Z^{<e>} = \left(\frac{i\omega\cdot\rho_0 A^2}{-\omega^2 m_p + i\omega b_p + k_p}\right)^{<e>} \quad (21)$$

In case an inviscid fluid is considered the relevant parameters simplify to $\Gamma(\omega) = i$ en $G(\omega) = 1$. So, with (11), $\kappa = i\omega L/c_0$. The tube element matrix then changes in:

$$[K] = \frac{-iA}{\sin(\omega L/c_0)} \begin{bmatrix} \cos(\omega L/c_0) & -1 \\ -1 & \cos(\omega L/c_0) \end{bmatrix} \quad (22)$$

As can be seen the element matrix shows a singularity if ω becomes a multiple of $\pi c_0/L$, i.e. when an exact multiple of half-waves is present in the tube. It is recommended to avoid this choice of ω during a harmonic response calculation, or to employ always a viscothermal approach.
The above developed theory is implemented in a Matlab program and alternatively a MathCad sheet. In a FEM-like way the element properties and the nodal point topology are inserted. Boundary conditions are set and a system matrix and vector is drawn up. For a frequency range this system is solved and one or more harmonic response curves are determined. Obviously it is possible to distillate the (complex) eigenfrequencies of the system by finding the zero-points of the determinant of the system matrix.

References

[1] H. Bergh: A new method for measuring the pressure distribution on harmonically oscillating wings. Proc. 4 th ICAS Congress, Paris 1964 (eds: R. Dexter, Mac Millan Company, 1965).

[2] B. Laschka: Zur Theorie der harmonisch schwingenden tragender Flügel bei Unterschallanströmung. Z. Flugwissenschaften, Bd 11 (1963), p. 265 - 292.

[3] B. Laschka: Das potential und Geschwingkeitsfeld der harmonisch schwingenden tragende Fläche bei Unterschallströmung. ZAMM, Bd 43 (1963), p. 325 - 333.

[4] B. Laschka: Die Druck-, Auftriebs- und Momenten verteilungen an einem harmonisch schwingenden Flügel kleiner Streckung im niedrigen Unterschallbereich. Proc. 4 th ICAS Congress, Paris 1964 (eds: R. Dexter, Mac Millan Company, 1965).

[5] H. Bergh and H. Tijdeman: Theoretical and experimental results for the dynamic response of pressure measuring systems. NLR-TR F 238, 1965.

[6] H. Tijdeman: On the propagation of sound waves in cylindrical tubes. Journal of Sound and Vibration, 39 (1), p. 1 - 33, 1975.

[7] H. Tijdeman and H. Bergh: The influence of the main (cross) flow on the transfer function of tube-transducer systems used for unsteady pressure measurements. NLR - MP 72023 U, 1972.

[8] Hanno H. Heller and Sheila E. Widnall: Dynamics of a probe for measuring pressure fluctuations on a hypersonic re-entry vehicle. Journal Acoustic Society America, Vol 44, No. 4, 1968, p. 885 - 896

[9] Geoffrey P. Watts: personal communication. See also: The response of pressure transmission lines. 20th Annual ISA conference, October 1965, Los Angelos, paper 13.3 - 1 - 65.

[10] J.Ruud van Ommen, Jaap C. Schouten, Michel L.M. van der Stappen and Cor M. Van Beek: Response characteristics of probe transducer systems used for unsteady pressure measurements in gas-solid fluidized beds: how to prevent pitfalls in dynamic pressure measurements. Powder Technology, 106, (1999), p. 199 - 218.

[11] J.-F. Broukaert: Development of single and multi-hole fast response probes for turbomachinery applications. Proc. XV symposium on measuring techniques for transonic and supersonic flows in cascades. Firenze, Italy, 2000.

[12] C.H. Sieverdings, T. Arts, R. Denos, J.-F. Brouckaert: Measurement techniques for unsteady flows in turbo-machines. Experiments in Fluids, Vol. 28, No.4, April, 2000, p. 285 - 321.

[13] Tony R. Parrot, Michael G. Jones and Ernie M. Thurlow: Unsteady pressure loads in a generic high-speed engine model. NASA TP 3189, 1992

[14] Stephen A. Whitmore, Brian J. Petersen and David D. Scott: A dynamic response model for pressure sensors in continuum and high Knudsen number flows with large temperature gradients. NASA TM - 4728, 1996.

[15] P.A. Findlater, S.E. Greenhill and W.D. Scott: Design and testing of a turbulence probe for harsh flows. Environmental Fluid Mechanics 1: 3 - 28, 2001

[16] N. Rott: Damped and thermically driven oscillations. ZAMP, 20, 1969, p. 230 - 243.

[17] N. Rott: The heading effect connected with non-linear oscillations in a resonance tube. Journal of Applied Mechanics and Physics (ZAMP), Vol. 25, 1974, p. 619 - 634

[18] E. Rodarte, G. Singh, N.R. Miller and P. Hrnjak: Sound attenuation in tubes due to viscothermal effects. Journal of Sound and Vibration (2000) 231 (5), 1221 - 1242

[19] Z. Kazimierski and L. Horodko: Second order effects of oscillating gas in tubes of small diameter. Journal of Sound and Vibration (1993) 167(2), p. 317 - 329.

[20] J.-G. IH, C.-M. Park and H.-J. Kim: A model for sound propagation in capillary ducts with mean flow. Journal of Sound and Vibration (1996) 190 (2), p. 163 - 175.

[21] K.-W. Jeong and J.-G. IH: a numerical study on the propagation of sound through capillary tubes with mean flow. Journal of Sound and Vibration (1996) 198(1), 67 - 79

[22] W.M. Beltman: Viscothermal wave propagation including acousto-elastic interaction. PhD-thesis, ISBN 90-3651217-4, University of Twente, 1998.

[23] W.M. Beltman: Viscothermal wave propagation including acousto-elastic coupling. Journal of Sound and Vibration 227 (3) 1999 part I: Theory p. 555 - 586, Part II: Applications p. 587 - 609.

[24] F.J.M. van der Eerden: Noise reduction with coupled prismatic tubes. PhD thesis, ISBN 90-36515211, University of Twente, 2000.

[25] F.J.M. van der Eerden, H. Tijdeman: Acoustic Impedance of coupled tubes, including viscothermal effects. Internoise 99, December 6 - 8, Fort Lauderdale, Florida, USA, 1999.

[26] D.A. Bies and C.H. Hansen: Engineering Noise Control. Second edition 1996, T J Press, Padstow, ISBN 0 419 20430 X

[27] H.E. de Bree, R.J. Leusink, M.T. Korthorst, H.V. Jansen, T. Lammertink, M.C. Elwenspoek: The Microflown, a novel device measuring acoustical flows, Sensors and Actuators, A, **54**, p. 552 - 557.

[28] M.E. Delany and E.N. Bazley, Applied Acoustics, **3**, p. 105 - 116, 1970.

[29] W.M. Beltman: P.J.M. van der Hoogt, R.M.E.J. Spiering, H. Tijdeman: Air loads on a rigid plate oscillating normal to a fixed surface. Journal of Sound and Vibration 206, p. 217 - 241, 1997

[30] W.M. Beltman, P.J.M. van der Hoogt, R.M.E.J. Spiering, H. Tijdeman: Implementation and experimental validation of a new viscothermal acoustic finite element for acousto-elastic problems. Journal of Sound and Vibration 216(1), p. 159 - 185, 1998.

[31] T.G.H. Basten: Noise reduction by viscothermal acousto-elastic interaction in double wall panels. PhD thesis, ISBN90-365-1597-1, 2001.

[32] T.G.H. Basten, P.J.M. van der Hoogt, R.M.E.J. Spiering, H.Tijdeman: On the acoustic-elastic behaviour of double-wall panels with a viscothermal air layer. Journal of Sound and Vibration, 243,(4), p. 699 - 719, 2001.

[33] T.G.H. Basten and H. Tijdeman: Damping of structural vibrations by vortex shedding. ISMA 25, International Conference on noise and Vibration Engineering, p. 287 - 294, Leuven, Belgium, 2000.